UNIVERSITÉ DE GENÈVE

Archive ouverte UNIGE
https://archive-ouverte.unige.ch

Article scientifique | Article | 2013

Accepted version | Open Access

This is an author manuscript post-peer-reviewing (accepted version) of the original publication. The layout of the published version may differ .

Summer comfort in a low-inertia building with a new free-cooling system

Brun, Adrien; Wurtz, Etienne; Quenard, Daniel; Hollmuller, Pierre

How to cite

BRUN, Adrien et al. Summer comfort in a low-inertia building with a new free-cooling system. In: Applied energy, 2013, vol. 112, p. 338–349. doi: 10.1016/j.apenergy.2013.05.052

This publication URL: https://archive-ouverte.unige.ch/unige:34583
Publication DOI: 10.1016/j.apenergy.2013.05.052

© This document is protected by copyright. Please refer to copyright holder(s) for terms of use.

Published in: Applied Energy 112 (2013) 338–349
http://www.sciencedirect.com/science/article/pii/S0306261913004649

Summer comfort in a low-inertia building with a new free-cooling system

A.Brun[a], E.Wurtz[a], D.Quenard[b], P.Hollmuller[c]

[a] *LEB - CEA - INES, 50 av du lac Leman, Le Bourget du Lac, France*
[b] *Centre Scientifique et Technique du Btiment, 24 rue Joseph Fourier, 38400 St-Martin d'Hères, France*
[c] *Institut des Sciences de l'Environnement, Groupe Energie, Université de Genève, 7rte de Drize, CH - 1227 Carouge, Suisse*

Abstract

Wood-framed buildings are considered to have low energy consumption since their construction mode generally gives high U-values and limited thermal bridges. Although the construction mode results in low heating consumption, the lack of storage capacity in the internal walls makes passive cooling designs such as night ventilation inappropriate. Consequently, the interior is subject to considerable temperature swings and higher temperatures than those of buildings with more massive internal surfaces. This paper investigates the possibility of reducing the energy used for cooling buildings by linking a so-called "phase-shifter" air/mass system to the HVAC system. This system is capable to restore the night cooling potential in the daytime by shifting the input temperature oscillation to around half a day, whereas temperature swing is conserved. The numerical model implemented on the SimSpark platform has been validated against the analytical solution for the constant airflow and harmonic temperature profile; then experimental data (obtained from the full-scale prototype designed and installed at the CSTB) has been used to assess its predictive capability with non-constant airflow. Using reduced ventilation periods has been numerically studied regarding environmental air resource and thermal storage efficiently of the system. The size and electricity consumption were optimized by this way. A comfort analysis was carried out on an experimental building with very high energy efficiency (INCA, INES, Le Bourget-du-Lac, France) based on the EN ISO 15251 adaptive model. Energy building simulations demonstrate that associating a phase-shifter to a low-inertia building gives it similar internal conditions to those of a more massive night-ventilated structure. Furthermore the proposed optimization greatly reduces the size of the system (by 30%) and the electricity consumption (by at least 38%) while the temperature is out of the comfort range for an extra 5% of the time.

Keywords: thermal mass, phase-shift, summer comfort, low-inertia building

Email address: Contact : adrien.brun@cea.fr/ Tel : +33 675 545 260 / Fax : +33 479 688 049 (A.Brun)

1. Introduction

Using wood-based building systems presents lower life-cycle primary energy balances than thermally equivalent steel or concrete-based building systems [1, 2]. Such building system, characterized by a low thermal inertia and thermal bridge, is widely used in cold-climat while passive energy storage through high thermal mass not significantly change the energy consumption [3]. However in mild to hot-climates, prevent overheating in passive building is a big concern. Passive cooling techniques could hence be used in order to achieve comfortable internal condition while keeping energetic cost to the minimum. Such techniques have been classified by Givoni [4] according to the natural source from where the cooling energy is derived: evaporative, soil and ventilative techniques. Artmann et al. [5] and in a more recent work Chesne et al. [6] have defined environmental resources indicators in order to quantify the ability of the air resource to cover the cooling energy needs of a building. Results show a significant potential in Central, Eastern and some region of Southern Europe. Unfortunately, such strategy is not suited to lightweight buildings. Their low thermal storage makes nocturnal ventilative cooling strategies not appropriate as they don't significantly lower the maximal temperature and they increase the day/night temperature difference [7].

A lot of published literature is available regarding passive or free-cooling techniques. Those specifics to lightweight building consist in introducing thermal storage material in the structure. As examples, replacement of the standard wallboard by one's containing phase change material (PCM) has been widely studied [8, 9, 10]. Fraisse et al. [11] studies active ventilation inside air gap of a double wall with high thermal inertia. Other techniques remained the structure of the building unchanged but storing and extracting the cold needed electric fan. As an alternative of positioning the thermal mass in the walls, it could be introduced into the ventilation system. Heat thermal energy storage unit (HTES) is a similar free-cooling system to the one studied in this paper. Storage medium could be in the form of latent and sensible energy type [12, 13, 14] or solely sensible [15]. Earth-to-air heat exchanger (EAHE) is also introduced in the building HVAC system and act as a pre-heating and free-cooling unit. According to the classification of Givoni [4], EAHE differs from HTES by the source of energy. The main defects of the EAHE from HTES are the areas of land it occupies, the cost of the installation, vapor condensation discharge from EAHE and possibility of fatal microorganisms cultivate [16].

The research proposed here differs from previous work on heat thermal energy storage unit and summer comfort in lightweight building's from:

- The so called "phase shifter" is a new type of HTES that allows shifting the temperature oscillation half-day with almost no dampening [17]. This system has been seldom studied so far.
- We studied the behavior of the system when the airflow was intermittent. The impacts of the type of operating mode on its dimensions as well as the reported cooling potential were quantified.
- The coupling of the system with a lightweight building was simulated to evaluated the service provided in both operating mode. Their behaviors were compared to that of a heavy building ventilated at night.

In the following introduction we illustrate the principe of the "phase-shifted ventilation" and the two-phase Schumann model.

//Figure1//

The aim of 'phase-shifted ventilation' system is to delay the input temperature signal without dampening it, Fig.1. System affects the temperature oscillation by a time-shift (ϕ) with a transmission factor (τ) close to 1. The physical phenomena that take place in a thermal phase-shifter are similar to those in a packed bed. The system schematic is given in Fig.2. It is entirely defined by:

- A mechanically induced airflow $\dot{m}_a$ at temperature T_a passes through storage elements of volume V_m and exchange. surface S_m that are homogenously distributed within a duct with section S, length L and volume $V = L \times S$.
- The void fraction defined as $\eta = (1 - V_m/V)$.
- The volume of air on filled duct, $V_a = \eta V$.
- The equivalent thickness of the storage element $r_m = V_m/S_m$.
- Constant airflow, duct section and void fraction which yields the free and interstitial velocities v_o and v.
- A unitary exchange surface $s_m = S_m/L$.
- The convective heat exchange between air and storage material, h_o.
- The unitary periodic storage capacity, $k_o = \omega C_{p_m} \rho_m r_m$.
- Air specific thermal capacity C_{p_a} , air mass per volume ρ_a, material specific thermal capacity C_{p_m} and material mass per volume ρ_m.

//Figure2//

The two-phase model is based on the following assumptions:

- Temperature in each storage element T_m is homogeneous (lumped capacity model).
- The arrangement of the storage elements, airflow and convective coefficient are independent of the cross-section and along the length of the system.
- Axial heat transfer is negligible.
- The ducting is totally adiabatic.

These assumptions lead to the two-phase Schumann model [18] in which the energy balance on air and on material is represented by the following equations:

$$C_{p_a} \dot{m}_a \left(\frac{1}{v} \delta_t T_a \right) + s_m h_o \left(T_a - T_m \right) = 0 \tag{1}$$

$$r_m C_{p_m} \rho_m \delta_t T_m + h_o \left(T_m - T_a\right) = 0 \tag{2}$$

In the case of harmonic excitation $\left(T_{ps|_{x=0}}(t) = A\cos(\omega t)\right)$, Hollmuller et al. [19] proposes a solution in a permanent regime, where $T_{ps|_x}$ gives air temperature at distance x from the system inlet and A the amplitude of the harmonic signal :

$$T_{ps|_{x=L}}(t) = A\exp\left(\frac{-hs_m L}{C_{p_a}\dot{m}_a}\right)\cos\left(\omega\left(t - \frac{L}{v}\right) - \frac{ks_m L}{C_{p_a}\dot{m}_a}\right) \tag{3}$$

$$\text{with} \quad \begin{cases} h = h_o k_o^2 / \left(h_o^2 + k_o^2\right) \\ k = h_o^2 k_o / \left(h_o^2 + k_o^2\right) \end{cases} \tag{4}$$

For common storage material with high capacity compared to air ($Cp_a\rho_a \ll Cp_m\rho_m$) and low unitary periodic storage capacity in relation to convective exchange ($k_o \ll h_o$), phase-shift and amplitude-transmission are expressed as:

$$\tau \approx \exp\left(-\frac{k_o}{h_o}\phi\right) \quad \text{and} \quad \phi \approx \frac{ks_m L}{C_{p_a}\dot{m}_a} \tag{5}$$

Currently, very few studies [20, 21] deal with the interest of linking this system to the building and almost consider a continuous mechanically induced airflow. As will been seen in the article, numerical solution of the Schumann model yields very satisfying results with non-continuous airflow and non-harmonic temperature oscillation. Continuous and intermittent system ventilation modes have then been tested on a low-inertia building.

2. Description and validation of the numerical model

2.1. SimSpark implementation

To assess the energy behavior of the system with no constant airflow and no harmonic solicitation, the Schumann model can be solved numerically by using the finite volume method with the solver Spark [22]. Equations for the i^{th} control volume are as follows:

$$C_{p_a}\dot{m}_a\left(T_{e_i} - T_{s_i}\right) = S_m h_o\left(T_{a_i} - T_{m_i}\right) + \rho_a C_{p_a} V_a \delta_t T_{a_i} \tag{6}$$

$$S_m h_o\left(T_{a_i} - T_{m_i}\right) = \rho_m C_{p_m} V_m \delta_t T_{m_i} \tag{7}$$

$$T_{a_i} = \left(T_{e_i} - T_{s_i}\right)/2 \tag{8}$$

T_{e_i} and T_{s_i} represent respectively the inlet and the outlet air temperature of the i^{th} control volume, $T_{a_i}$the mean air temperature and $T_{m_i}$the particle temperature. The system model consists of 14 control volumes coupled together ($T_{s_{i-1}}$=T_{e_i}). The variables and parameters of the model are: T_{ext}, P_{atm}, H_r, Q_v, ρ_m,Cp_m, h_o, η, V_a, V_m, S_m, S, L. Relations between spherical storage elements characteristics (R, η) and equations parameters are as follow : $S_m = 3LS(1-\eta)/R$, $V_a = \eta SL$ and $V_m = (1-\eta)SL$.

2.2. Numerical versus analytical solutions

To confirm that the implementation is correct and the discretization is sufficient, the model was compared to the analytical solution (Eq.(4)) after an initialization period of 10 days. The validation concerns the outlet air temperature in the case of harmonic excitation ($T_{ps|_{x=0}}(h) = A\cos(2\pi(h - cst)/24) + \overline{T_{ext}}$) and constant airflow. The benchmark between an analytical and a numerical solution was realized for a large input domain. Constant parameters are as follow : $C_{p_a} = 1000\ J\ kg^{-1}\ K^{-1}$, $\rho_a = 1.12\ kg\ m^{-3}$,$C_{p_m} = 4180\ J\ kg^{-1}\ K^{-1}$, $\rho_a = 1000\ kg\ m^{-3}$, $R = 0.00475\ m$, $S = 0.5\ m^2$,$\eta = 0.34$, $\overline{T_{ext}} = 23\ ^oC$ and $A = 9\ ^oC$. Phase-shifting and amplitude transmission were compared for airflow rates of between 100 and 400 $m^3\ h^{-1}$ and material volume between 0.5 and 1.75 m^3 (the Achenbach correlation [23] links the convective exchange to the airflow rate). Fig.3 compares analytical and numerical air outlet solution for 350 $m^3\ h^{-1}$ airflow rate and 1.75 m^3 material volume. For the various airflow and material volume combination, it has been found that the differences in terms of transmission amplitude and phase-shift do not exceed 5%, with the maximum occurring for low amplitude signals. For these reasons the accuracy of the numerical model in the specific case of harmonic excitation is considered to be in satisfactory agreement with the analytical solution.

//Figure3//

For the analytical/numerical comparison, numerical solving was carried out with a short time-step calculation (1 minute). In order to compute energy simulation on a large time-scale with a reasonable calculation cost, sensitivity of this parameter on the output temperature was evaluated for time steps of 1, 5, 15 and 30 minutes and 1 hour. The simulations have shown that the differences in all time-solving resolutions are lower than 0.2 ^oC. Model validity was further investigated with non-constant airflow using the prototype presented below.

2.3. Prototype description

//Figure4//

The CSTB prototype (Fig.4) differs from models of previous experiments [19] in three main ways. The first is that the airflow rate can be made time-dependent; the second concerns the structure and dimensions of the duct that allows the use of material in sufficient quantities to enable phase-shifting of greater than 8.00 h, considering an airflow rate of 250 $m^3\ h^{-1}$. Finally, the system is designed for external use and so it could be easily coupled to a small building or test cell. The prototype consists of a duct which is 4.5 m in length and $1.1 \times 0.6\ m$ in cross-section with 20 cm of polystyrene insulation around it. A fan provides the airflow and the rate can be controlled with a $0-10\ V$ signal. Water was chosen as the material due to its high sensible heat, which can reduce the required quantities by 40% **?**]; water is held in a 10 cm diameter polyolefine ball (Cristopia nodules). The duct was filled with 2200 nodules in a compact hexagonal arrangement occupying 1.25 m^3, so the void fraction was approximately 0.34. We carried out experimentation over several weeks with an airflow of 380 $m^3\ h^{-1}\ m^{-2}$. Temperature along the channel (air and surface material), airflow rate at the outlet and pressure

losses in the packed bed were measured with a Campbell data logger. Transmission and phase-shift were deduced from a Fourier series analysis on temperature measurement. We obtained a transmission of 33% and a phase-shift of 11 h. Compared to the 80% transmission obtained with the 16/13 PVC tubes placed perpendicularly to the airflow, the 33% transmission is not satisfactory **(Ajouter la reference pour les tubes PVC)**. Reducing the diameter of the nodules may enhance the transmission by increasing the ratio between convective exchange and unitary periodical storage capacity ($h_o < k_o$) (cf. Eq.(5)) but these nodules are not produced in a smaller size. Despite a lower than expected transmission, the experimental set-up was able to assess the validity of the numerical model for intermittent airflow circulation.

2.4. Experimental validation

The first step was to calibrate the model parameters for permanent airflow circulation. Fig.5 represents the comparison of experimental and numerical output temperature after the calibration step. Two parameters were chosen - the convective heat transfer coefficient (h_o) and the system length (L). Calibration was obtained by minimizing the quadratic error between experimental and numerical output temperature using GenOpt [24]. The value of the convective heat transfer resulting from the optimization was 11.8 $W\ m^{-2}\ K$ and the volume corresponding to the system length was 0.92 m^3 - a reduction of 27% compared to the real volume. This difference may be due to the non-homogeneous airflow in the section and along the axis. Furthermore, the experimental result revealed that 24 hours are needed to initialize the dynamic variables (air and particle temperatures), after which only small differences (less than 0.5 ^oC) persist.

//Figure5//

In the second step, we were mainly interested in assessing the validity of our model for alternated airflow circulation (alternating 6 h periods with and without ventilation). The previously calibrated model was used unchanged and the airflow pattern was the same as the experimental one. The comparison between experimental and numerical outlet temperature is shown in Fig.6. The precision in the case of intermittent ventilation is comparable to that obtained with a constant airflow rate; one difference concerns the dynamic variables initialization times that take approximately 48 h.

//Figure6//

In the numerical model, the energy conservation law indicates that with the airflow rate at zero, the material temperature remains constant. Fig.7 shows nodule temperature at different distances from the air inlet: 25, 75, 125, 175, 225, 275 and 325 cm. These temperatures were recorded between the 20 and 26 August 2010. In this period, ventilation was stopped at noon on the 21 August; from that moment, the temperature presented dampened daily oscillations on the entry and the exit section due to air infiltration, while the other temperatures moved away from their initial values by only 2 ^oC on a five-day sequence. This limited temperature variation over a sequence of five days shows that the model assumption - that material temperatures are constant during ventilation stop periods of less than 10 hours - is acceptable.

//Figure7//

3. Thermal storage efficiency under intermittent ventilation

To assess the behavior of the system under intermittent ventilation, parametric studies on storage volume and ventilation cycle duration were conducted for three systems distinguishable by their transmission amplitude. The best one transmits 72% of the initial signal amplitude while the lower amplitude transmission considered was equivalent to our prototype (32%). The evaluation criterion is the thermal storage efficiency (η_{ps}), which is given by the fraction of the reported cooling potential (RCP) over the available daily cooling potential (DCP). The cooling energy is assumed to be reported as long as the output temperature is inferior to the reference and to the outside temperature. Fig.8 gives a graphical explanation of the calculation method.

//Figure8//

Parametric simulation and post-treatment were carried out using Matlab as well as the SimSpark simulation platform. For each system, the quantity of material and convective heat transfer were fitted to achieve a complete phase-shift (12 h) and defined transmission amplitude considering Cristopia nodules as storage material, and a 0.34 void fraction. The multiple simulations were carried out over the month of June considering the meteorological data of Grenoble.

//Figure9//

Fig.9 shows twenty thermal efficiency curves; each of the curves represents a specific ventilation cycle that we characterize by the daily duration of ventilation, which is of between 8 h 50 min and 24 h. To go from one curve to the next, one adds 2 h25 min of ventilation. Each of the curves represents a specific ventilation cycle that we characterize by the daily duration of ventilation. For continuous ventilation (the black curve), reduction of the initial storage volume (V_{init}) to half of its initial value reduces the storage efficiency from 96% to 54%. When the quantities of material are reduced, phase-shifting decreases linearly, whereas transmission increases exponentially (Eq.(5)). Despite the better transmission, reducing the phase-shifting considerably reduces the daily periods during which the temperature of the system outlet is lower than the exterior temperature.

The ventilation periods are based on the times of minimum and maximum daily temperature. The thick grey curve is the thermal storage efficiency characteristic for 8 hours ventilation, by day and night. It has a parabolic profile with a maximum occurring at approximately 65% of the initial storage volume. The thermal storage efficiency is 20% higher than in the case of continuous ventilation.

An interesting result is that the reduction of the material storage quantities must be associated with a reduction in the ventilation duration to avoid a considerable reduction of the thermal storage efficiency. Reduction of the ventilation duration is interesting as it allows the daily ventilation to be fitted to the building load profile and the night ventilation to the environmental resource availability.

4. System integration in low-inertia buildings

4.1. Description of the method

Now, we use the system as an alternative or in conjunction with direct night ventilation for an office building in Chambery, France. First, we compare the thermal behavior of wooden and concrete night-ventilated structures. Then we try to minimize the hours of thermal discomfort by coupling the wooden building to the thermal phase shifter. Continuous and intermittent storage irrigation are tested and comfort analysis of the building is assessed according to several methods of comfort evaluation (Fanger EN ISO 7730, Adaptive approach EN ISO 15251, Givoni zones, ASHRAE summer zone). In the following, the four configurations are noted:

- C: Night-ventilated concrete structure,
- W: Night-ventilated wooden structure,
- W24: Identical to W but HVAC is associated with continually ventilated thermal storage requiring 3.4 m^3 of storage material,
- W16: Identical to W24 but ventilation duration is reduced from 24 $h/24$ to 16 $h/24$ and optimization of the η_{ps} leads to a reduction in the material quantity from 3.4 to 2.3 m^3.

The differences between C and W configurations are as follows:

- Inner wall layer: 15 cm heavy concrete instead of 1.3 cm plasterboard,
- First floor slab: 15 cm heavy concrete instead of 5 cm wood.

Year-round simulation was carried out using the meteorological data set of Chambery. For each simulation, the systems were pre-simulated for a continuous and an intermittent ventilation pattern using the numerical model presented. Building responses were then simulated within a SimSpark building model which integrates a ventilation control algorithm using the pre-simulated system as an input. The algorithm selects - among recovery ventilation, direct ventilation, night ventilation and phase-shifted ventilation - the most interesting mode according to the building variables (internal temperature, heating, temperature bounds) as shown in Fig.10. To improve the simulation accuracy, the time step was reduced to 5 min.

//Figure10//

4.2. Building test-case

The test case is shown in Fig.11. It is the wood-framed house on the INCAS experimental platform near Chambéry (France) whose complete description can be found in [25]. INCAS consists of 3 detached houses which have the same dimensions but different construction techniques. Each house contains more than 100 sensors to quantify and compare their thermal behavior and indoor air quality. This is a two-storey building with insulation ranging from 20cm (slab and vertical wall) to 40cm for the ceiling. Overhang

size and south windows surfaces have been optimized to reduce heating consumption and heat gain during the summer.

//Figure11//

Building energy simulation is effected using a building energy model developed in [26] under the SimSpark simulation environment [22]. The thermal model consists of two zones: the first and the second floors. The main parameters governing thermal behavior are as follows:

- External walls are considered as a single 20 cm layer of insulation. As result, the thermal inertia of the building is limited. Slab is the only concrete surface in the construction.
- The solar access is oriented 15 ^{o} southeast with a window-to-wall aera ratio of 28%. External solar shading is designed to minimize the solar gain in summer and maximize it in winter.
- The internal layout represents an office building with 15 W/m^2 internal gain in the $8:00-12:00$ h and $14:00-18:00$ h occupancy period, 5 W/m^2 between $12:00-14:00$ h and 3 W/m^2 between $18:00h-8:00$ h.

5. Results and discussion

5.0.1. Thermal behavior

//Figure12//

Fig.12 presents building energy simulations for the different configurations: ventilation modes for W24 and W16, the indoor temperature of the 4 configurations and the common internal load. Fig.13 shows the overheating duration for the year, considering periods of occupancy only (2600 $h/year$).

Temperature damping is relevant when a structure is made of high thermal storage material. On the second day of the presented sequence, the temperature amplitude was 11 ^oC in the wooden building and only 6 ^oC in the concrete structure. Consequently, the maximum temperature is limited to 28 ^oC in a massive building but reaches up to 31 ^oC in wooden structures. Cumulated overheating temperatures are more than two times lower in heavy structures for temperatures of up to 27 ^oC; this reflects the temperature damping capability of the thermal inertia. To conclude, low-inertia is characterized by fast response times and high temperatures, thermal comfort seems to be unacceptable and the building has to have a cooling system.

The association of the low-inertia structure to the sensible storage unit results in a thermal behavior similar to that of a heavy construction, with a reduction in amplitude and maximum temperature. Continuous system ventilation gives temperatures that are lower by 2 ^oC during the morning occupancy period and by more than 1 ^oC in the afternoon as compared to the high-inertia structure. In the case of intermittent ventilation, system ventilation starts at noon, when the wooden building temperatures reach the temperature of the concrete building. From that time, the system provides enough

fresh air to give a lower internal temperature than that of the concrete building. Fig.13 presents overheating cumulated temperature considering occupancy hours. For temperatures higher than 27 ^oC, the distribution provided by the intermittent system is identical to that of the continuously ventilated system.

//Figure13//

5.0.2. Comfort analysis

Comfort is evaluated for the summer period and only for the time of occupancy (Monday $\rightarrow$ Friday, 8 : 00 to 12 : 00 and 14 : 00 to 19 : 00) using four different comfort evaluation methods: the international standard EN ISO 7730 [27], the European standard EN ISO 15251 [28], the American standard ASHRAE [29] and the bio-climatic approach proposed by Givoni [30], all presented on a single psychometric chart.

- EN ISO 7730: the conventional comfort model, with a physical approach, involves the assumption that comfort can be derived from a human heat balance. The comfort bounds are derived from the PMV and PPD equations which represent the *"Predicted Mean Vote"* and *"Percentage of Persons Dissatisfied"* at less than 6 and 15% respectively. They are based on a summer clothing level (clo=0.5) and metabolism corresponding to a seated person ($1met \Leftrightarrow 58W/m^2$). The mean comfort temperature is approximately 25.5 ^oC with 0.5 ^oC tolerance, beyond which discomfort is assumed to occur for $PPD < 6\%$ and 1.5 ^oC tolerance for $PPD < 15\%$.

- ASHRAE Standard 55 also has a physical approach; the summer comfort zone specifies the conditions where sedentary or slightly active persons would feel slightly cool or warm ($\pm$ 0.5 on the ASHRAE thermal sensation scale). The comfort temperature range is about the same as the one obtained from the EN ISO 7730 with $PPD < 15\%$ but the mean comfort temperature is one degree lower.

- EN ISO 15251 is an empirical approach dedicated to buildings that have no mechanical cooling to reduce indoor temperatures. It introduces a consideration of the experience of the environment since the comfort temperature is calculated according to the previous daily mean temperature ($T_{rm} = (1-\alpha)(T_{ed-1} + \alpha T_{ed-2} + \alpha^2 T_{ed-3} + \cdots)$. The comfort temperature range is calculated as follows: $T_{bound} = 0.33 \times T_{rm} + 18.8 \pm Cat$, where Cat represents the interval tolerance (Category I: Cat=2, Category II: Cat=3, Category III: Cat=4).

- Givoni bio-climatic charts were developed by Givoni in 1976 and are based on indoor temperature (differing from Olgyay's charts which are based on external temperature) and defined climatic conditions under which various building design can provide indoor summer comfort: daytime ventilation, high mass, direct evaporation cooling and indirect evaporation cooling. The presented charts concern comfort acceptance in high-mass design strategies considering developed and hot developing countries.

The four comfort evaluation methods are reported in Fig.14 where each psychometric graph presents indoor temperature/humidity for the occupancy period from 1 June to 1

September. The graphics (a-b) concern the night ventilation strategy for the high-inertia building (the reference) and the wooden building. Overheating hours (EN15261 not respected), indicated by grey crosses, clearly appear for the wooden structure whereas almost all thermal responses of the concrete structure are included in the larger Givoni Chart. Coupling the low-inertia structure with the phase-shifting system gives satisfactory results since the number of overheating hours decreases considerably. Summer comfort provided by the continuous and the intermittent ventilation are graphically similar, so the adaptive comfort acceptance (expressed as a percentage of time) is proposed in Table 1.

//Figure14//

The following conclusion can be drawn from the comfort adaptive analysis:

- As previously indicated, the percentage of time during which comfort was not achieved in the wooden building is considerable; it reaches 59% of the occupancy period whereas it is only 11% for the high-mass structure, whose indoor climate could be classed half of the time in the first category.
- The unsatisfactory period falls from 59% to 17% when W building is coupled to the storage system. With the phase-shifting system, it is possible to achieve comparable comfort conditions as to those of the concrete building: Cat1 (C: 48%, W24: 45% W16: 41%), Cat2 (C: 23%, W24: 26% W16: 25%) and Cat3 (C: 18%, W24: 16% W16: 16%).
- The reduction of the ventilation duration by 38% has only a slight consequence on comfort: Cat1 (W24: 45% W16: 41%), Cat2 (W24: 26% W16: 25%) and Cat3 (W24: 16% W16: 16%) while contributing to at least a 38% reduction in electricity consumption and a 30% reduction in the size of the system.

//Table1//

It has been shown that the thermal phase-shifter system significantly improve the summer thermal comfort of the low-inertia structure without modifying any specificities of the wooden construction. From this combination (weighing $340 + 30\ kg\ m^{-2}$) results a temperature, distribution and comfort analysis that is not very different from the concrete one (weighing $1300\ kg\ m^{-2}$). Our optimized system shows that we could take best advantage of the conventional phase-shifter by greatly reducing its size (30%) and electricity consumption (at least 38%).

6. Conclusion

The two-phase model, usually analytically solved, was presented and numerically solved using the Spark solver. The model was validated according to the analytical model for harmonic solicitation and, for intermittent airflow, the model prediction availabilities were assessed and compared to the experimental output temperature, considerable agreement being noted.

So, the numerical model was used to assess the ability of the system to report the night potential for 140 combinations of ventilation duration and material storage size. One interesting result was that the thermal storage efficiency could be significantly improved by associating the reduction of the ventilation period with a reduction in the quantity of storage material. In other words, appropriate functioning periods could maintain high efficiently levels when the size of the system has to be reduced.

In the final part, a continually irrigated and an intermittent ventilated system were coupled to a low-inertia building and their thermal behavior was compared to a building that was identical except for its concrete structure. Our proposition consists of limiting the use of the system to periods when environmental potential and building cooling needs are at their maximum. It permits a considerable reduction in the size (more than 30%) and electricity consumption of the system and gives performances that are close to those of the high-inertia building.

While the optimization of a continuously ventilated phase-shifted system was mainly based on the determination of the optimal time-shifting and airflow rate as described in the first section, an optimal intermittent ventilation pattern is a complex optimizing process since it involves a time-variable parameter (airflow rate). In this work, ventilation start and stop times were scheduled and the output temperature of the system was pre-processed and used as input to the building thermal model, so the intermittent results do not correspond to the optimal possibility but are still of great interest. This optimization process will be part of further work involving coupled building and system equation solving and additional storage model validation for variable airflow rates.

7. Acknowledgements

This research was possible thanks to the contributions of the French Environment and Energy Management Agency (ADEME) and the Scientific and Technical Centre for Building (CSTB).

8. Nomenclature

DCP	Daily cooling potential	($^oC\ h$)
EAHE	Earth to air heat exchanger	
HVAC	Heating, ventilation and air-conditioning	
HTES	Heat thermal energy storage	
PCM	Phase change material	
PPD	Predicted percentage of dissatisfied	(%)
PMV	Predicted mean vote	
RCP	Reported cooling potential	($^oC\ h$)
Subscripts		
Mathematics		
$\overline{Y}$	Y means value	
$\delta_x Y$	Partial derivative of Y of variable x	

9. References

[1] B. Upton, R. Miner, M. Spinney, L. S. Heath, The greenhouse gas and energy impacts of using wood instead of alternatives in residential construction in the United States, Biomass Bioenerg 32 (1) (2008) 1–10, ISSN 0961-9534, doi:10.1016/j.biombioe.2007.07.001.

[2] A. Dodoo, L. Gustavsson, R. Sathre, Effect of thermal mass on life cycle primary energy balances of a concrete- and a wood-frame building, Appl Energy 92 (2012) 462–472, ISSN 0306-2619, doi: 10.1016/j.apenergy.2011.11.017.

[3] J. Karlsson, L. Wadso, M. Oberg, A conceptual model that simulates the influence of thermal inertia in building structures, Energy Build 60 (2013) 146–151, ISSN 0378-7788, doi: 10.1016/j.enbuild.2013.01.017.

[4] B. Givoni, Passive Low Energy Cooling of Buildings, John Wiley & Sons, ISBN 9780471284734, 1994.

[5] N. Artmann, H. Manz, P. Heiselberg, Climatic potential for passive cooling of buildings by night-time ventilation in Europe, Appl Energy 84 (2) (2007) 187–201, ISSN 0306-2619, doi: 10.1016/j.apenergy.2006.05.004.

[6] L. Chesne, T. Duforestel, J.-J. Roux, G. Rusaouen, Energy saving and environmental resources potentials: Toward new methods of building design, Build Environ 58 (2012) 199–207, ISSN 0360-1323, doi:10.1016/j.buildenv.2012.07.013.

[7] A. Brun, Amélioration du confort d'été dans des bâtiments à ossature par ventilation de l'enveloppe et stockage thermique, Ph.D. thesis, Université de Grenoble, 2011.

[8] D. Zhou, C. Zhao, Y. Tian, Review on thermal energy storage with phase change materials (PCMs) in building applications, Appl Energy 92 (2012) 593–605, ISSN 0306-2619, doi: 10.1016/j.apenergy.2011.08.025.

[9] F. Kuznik, D. David, K. Johannes, J.-J. Roux, A review on phase change materials integrated in building walls, Renew Sustain Energ Rev 15 (1) (2011) 379–391, ISSN 1364-0321, doi: 10.1016/j.rser.2010.08.019.

[10] G. Evola, L. Marletta, F. Sicurella, A methodology for investigating the effectiveness of PCM wallboards for summer thermal comfort in buildings, Build Environ 59 (2013) 517–527, ISSN 0360-1323, doi:10.1016/j.buildenv.2012.09.021.

[11] G. Fraisse, R. Boichot, J.-L. Kouyoumji, B. Souyri, Night cooling with a Ventilated Internal Double Wall, Energy Build 42 (3) (2010) 393–400, ISSN 0378-7788, doi:10.1016/j.enbuild.2009.10.007.

[12] A. Waqas, Z. Ud Din, Phase change material (PCM) storage for free cooling of buildings - A review, Renew Sustain Energ Rev 18 (2013) 607–625, ISSN 1364-0321, doi:10.1016/j.rser.2012.10.034.

[13] S. Decker, New passive solutions for summer comfort and timber housing in French Atlantic climate, Innsbruck, Austria, 2011.

[14] C. Arkar, B. Vidrih, S. Medved, Efficiency of free cooling using latent heat storage integrated into the ventilation system of a low energy building, Int J Refrig 30 (1) (2007) 134–143, ISSN 0140-7007, doi:10.1016/j.ijrefrig.2006.03.009.

[15] K. Dovrtel, S. Medved, Multi-objective optimization of a building free cooling system, based on weather prediction, Energy Build 52 (2012) 99–106, ISSN 0378-7788, doi: 10.1016/j.enbuild.2012.05.014.

[16] L. Ozgener, A review on the experimental and analytical analysis of earth to air heat exchanger (EAHE) systems in Turkey, Renew Sustain Energ Rev 15 (9) (2011) 4483–4490, ISSN 1364-0321, doi:10.1016/j.rser.2011.07.103.

[17] P. Hollmuller, Analytical characterisation of amplitude-dampening and phase-shifting in air/soil heat-exchangers, Int J Heat Mass Tran 46 (22) (2003) 4303–4317, ISSN 0017-9310, doi: 10.1016/S0017-9310(03)00199-6.

[18] T. Schumann, Heat transfer: A liquid flowing through a porous prism, J Franklin Inst 208 (3) (1929) 405–416, ISSN 0016-0032, doi:10.1016/S0016-0032(29)91186-8.

[19] P. Hollmuller, B. M. Lachal, J.-M. Zgraggen, A new ventilation and thermal storage technique for passive cooling of buildings: thermal phase-shifting, vol. 1, Geneva, Switzerland, 541–546, 2006.

[20] P. Hollmuller, P. G. Gallinelli, B. M. Lachal, W. Weber, Extensive sensitivity analysis of diverse ventilation cooling techniques for a typical administrative building in Mid-European climate, vol. 1, Lisbon, Portugal, 750–758, 2008.

[21] P. Hollmuller, J. Carlo, M. Ordenes, F. Westphal, R. Lamberts, Potential of buried pipes systems and derived techniques for passive cooling of buildings in Brazilian climates, vol. 1, Beijing, China, 329–336, 2007.

Table 1: Percentage of time when adaptive comfort (prEN15251) is achieved.

%	Cat1	Cat2	Cat3	Not respected
Concrete	48.0	23.5	17.8	10.7
Wood	24.8	9.3	7.2	58.7
Wood + 24h/24	45.4	26.1	16.1	12.4
Wood + 16h/24	41.4	24.8	16.4	17.5

[22] L. B. N. L. Simulation Research Group, Simulation Problem Analysis and Research Kernel (SPARK) reference manual, 2000.

[23] E. Achenbach, Heat and flow characteristics of packed beds, Exp Therm Fluid Sci 10 (1) (1995) 17–27, ISSN 0894-1777, doi:10.1016/0894-1777(94)00077-L.

[24] M. Wetter, GenOpt, Generic Optimization Program, Simulation Research Group, Lawrence Berkeley National Laboratory, 2008.

[25] C. Spitz, L. Mora, E. Wurtz, A. Jay, Practical application of uncertainty analysis and sensitivity analysis on an experimental house, Energy Build 55 (2012) 459–470, ISSN 0378-7788, doi: 10.1016/j.enbuild.2012.08.013.

[26] P. Tittelein, Environnements de simulation adaptés à l'étude du comportement énergétique des bâtiments basse consommation, Ph.D. thesis, Université de Savoie, 2008.

[27] EN ISO 7730, Ergonomics of the thermal environment, Analytical determination and interpretation of thermal comfort using calculation of the PMV and PPD indices and local thermal comfort criteria, 2005.

[28] EN 15251, Indoor environmental input parameters for design and assessment of energy performance of buildings addressing indoor air quality, thermal environment, lighting and acoustics, 2008.

[29] ASHRAE Standard 55/2004, Thermal environmental conditions for human occupancy, 2004.

[30] B. Givoni, Climate Considerations in Building and Urban Design, John Wiley & Sons, ISBN 9780471291770, 1998.

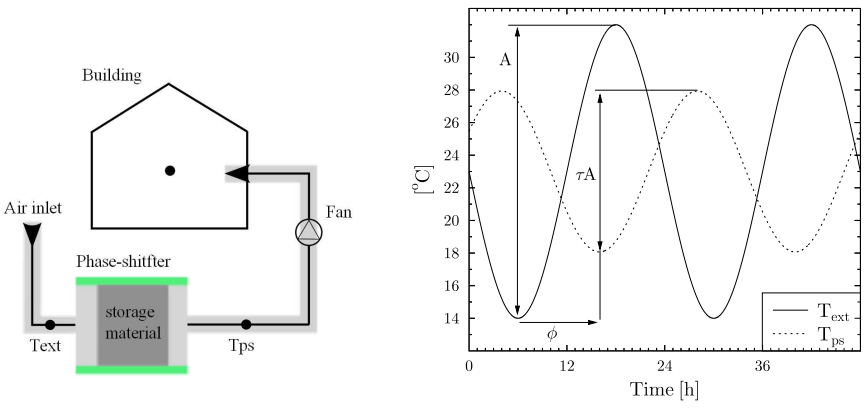

(a) (b)

Figure 1: Integration into the building ventilation system and day ventilation strategy (a), Input/output temperature profile over a 48h sequence (b).

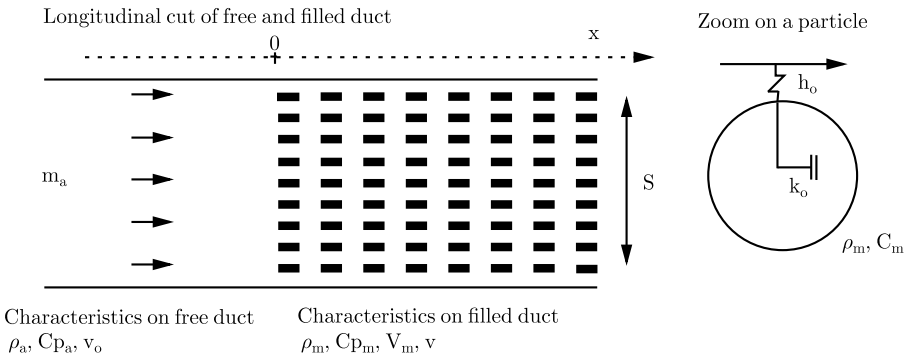

Figure 2: System schematic.

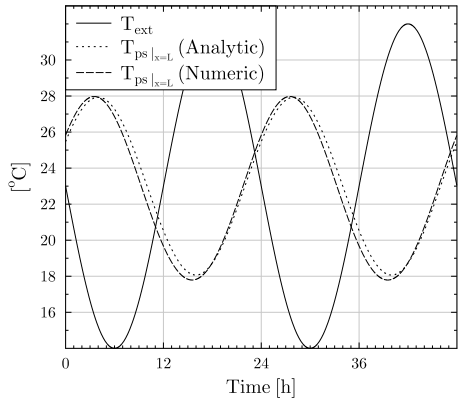

Figure 3: Analytic/numeric output temperature comparison.

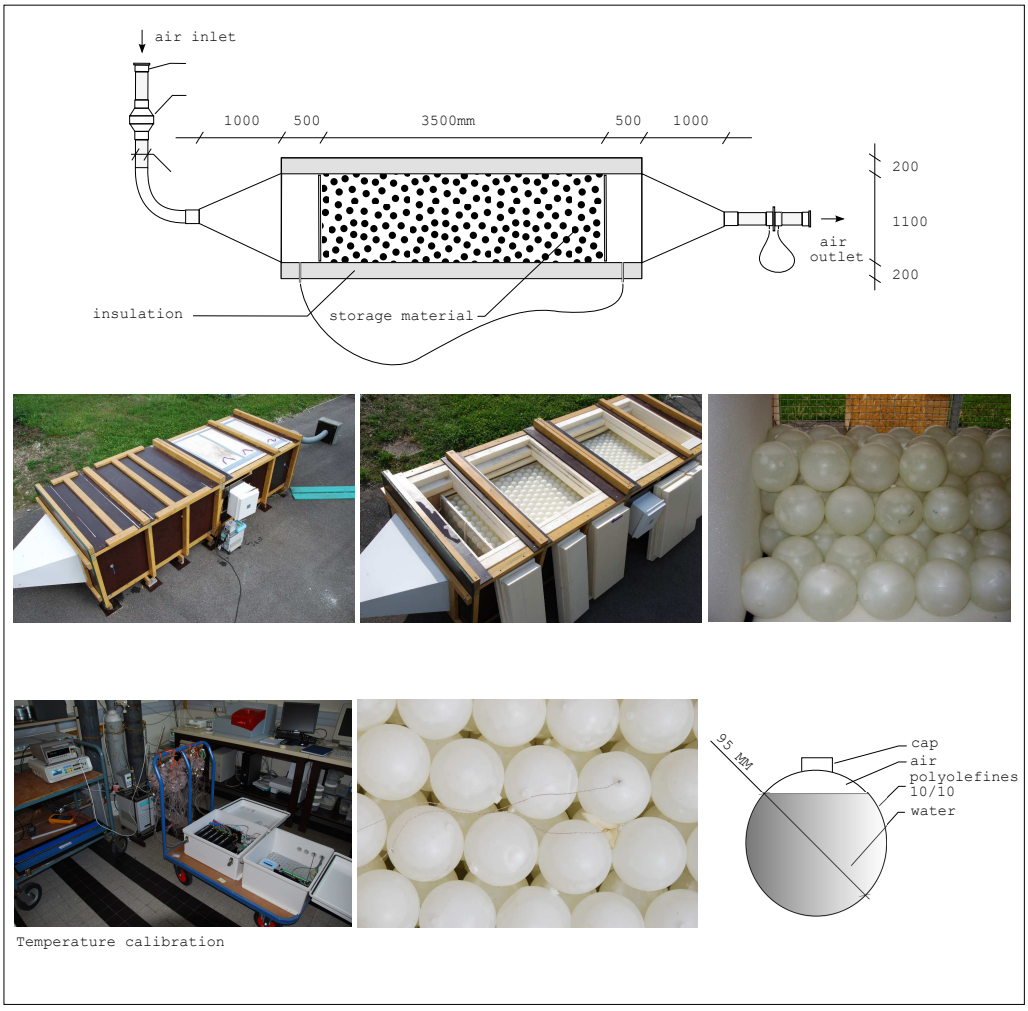

Figure 4: The CSTB prototype.

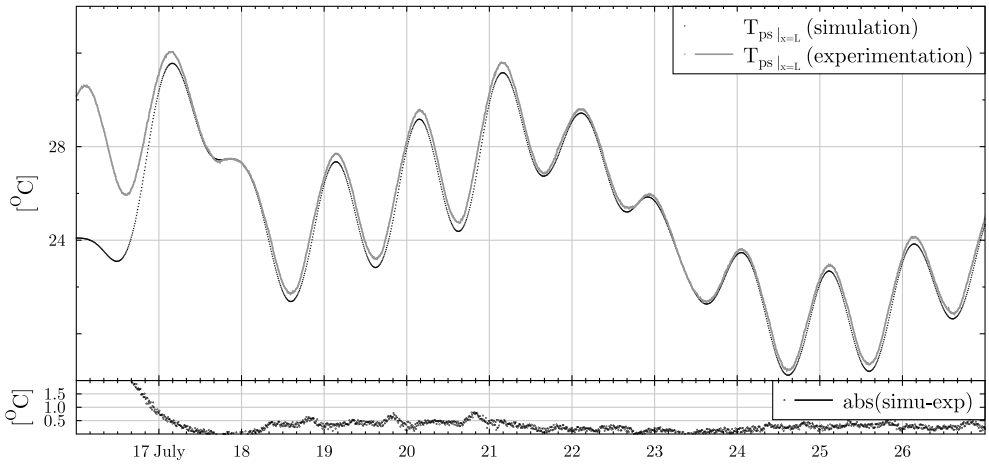

Figure 5: Comparison of experimental and numerical output temperature in continuous airflow ventilation.

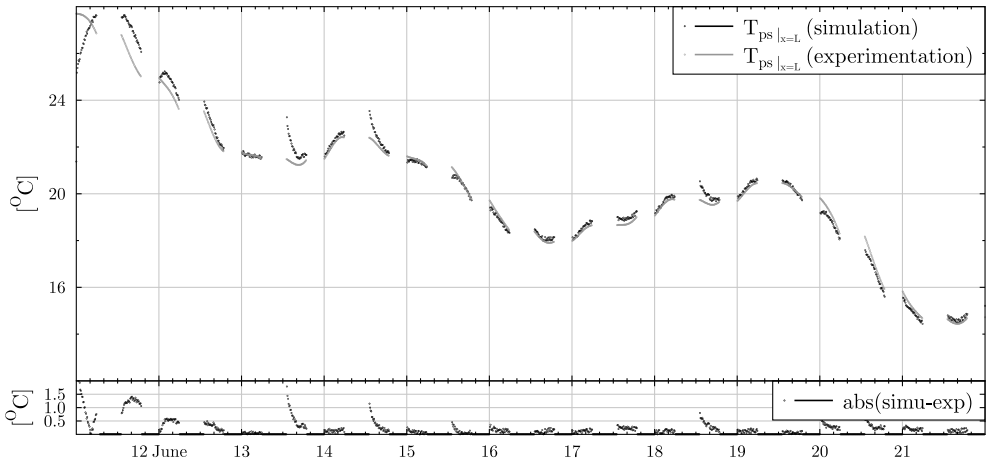

Figure 6: Comparison of experimental and numerical output temperature in non-continuous airflow ventilation.

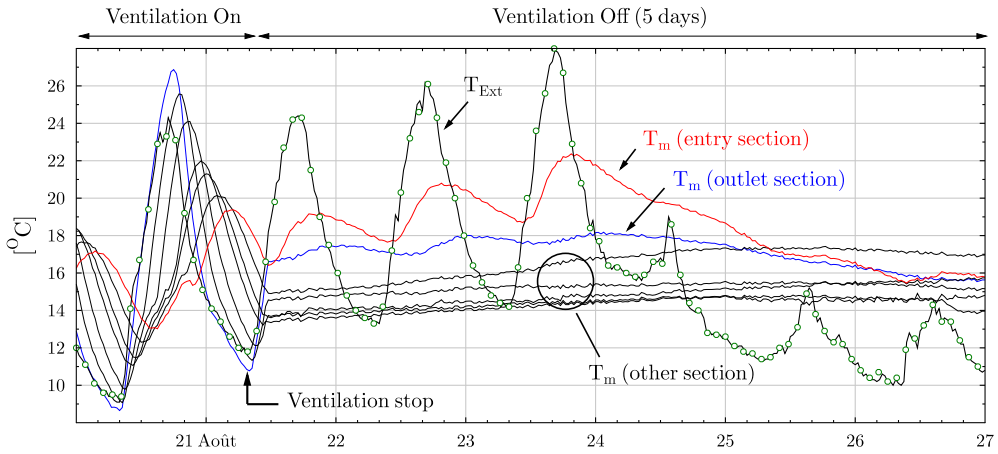

Figure 7: Nodule temperature variation when ventilation is stopped.

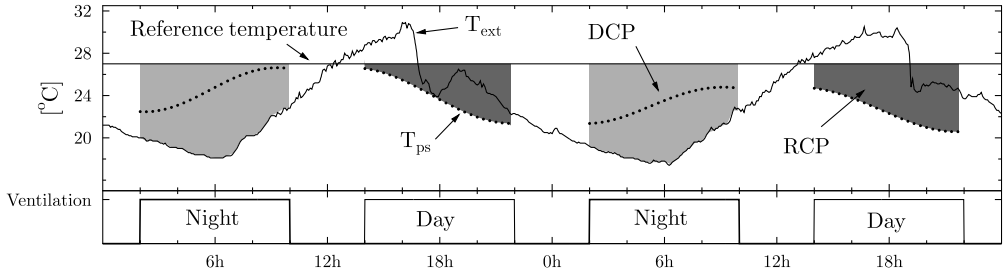

Figure 8: Thermal storage efficiency: calculation method.

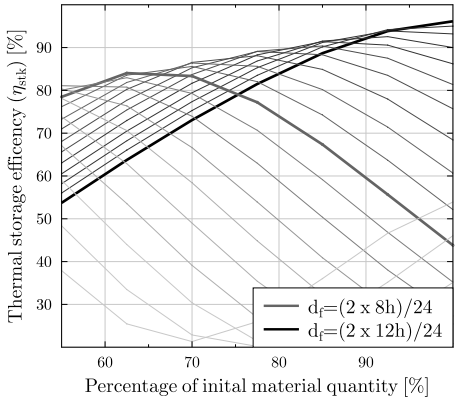

Figure 9: Mean thermal storage efficiency (η_{stk}) over the period from 30 June to 2 July 2010, Grenoble for the 72% transmission amplitude system with 27 ^oC as reference temperature (cf Fig.8), in function of the ventilation duration (d_f) and the percentage of initial storage volume (V_{init}).

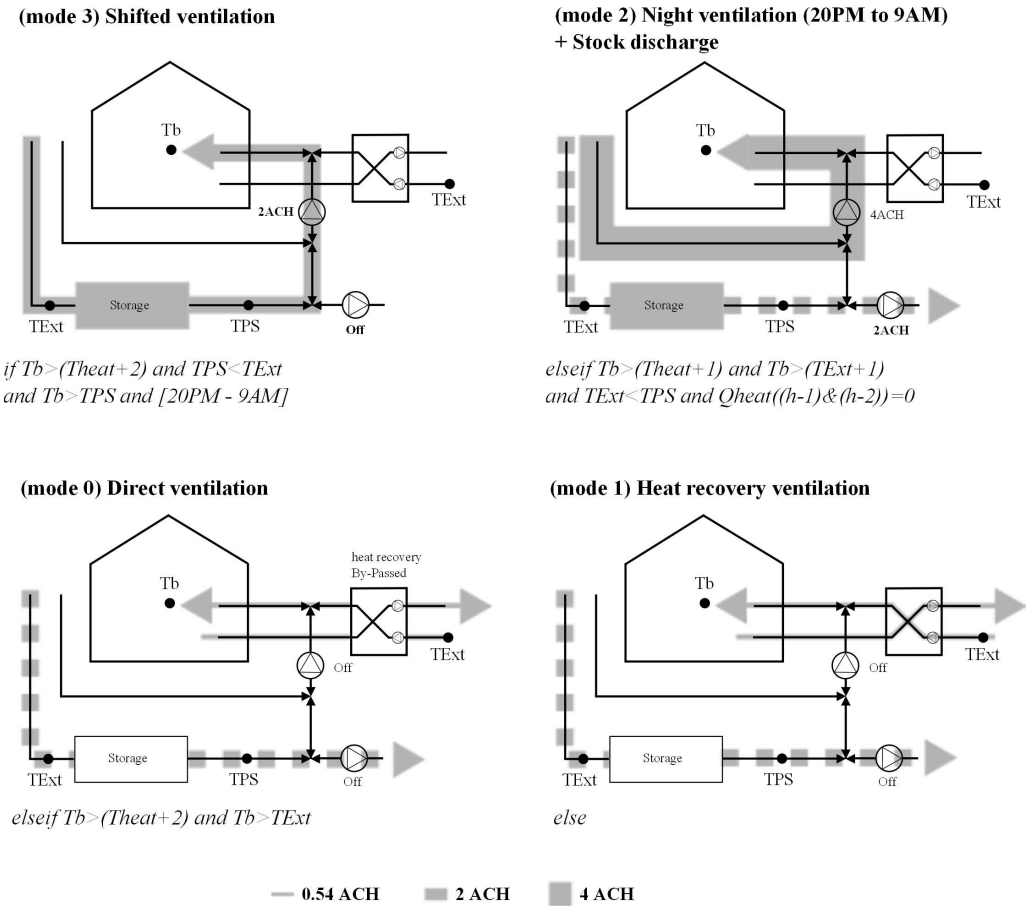

Figure 10: Different ventilation modes.

(a) (b)

Figure 11: Photography and 3D of one of the INCAS building test case.

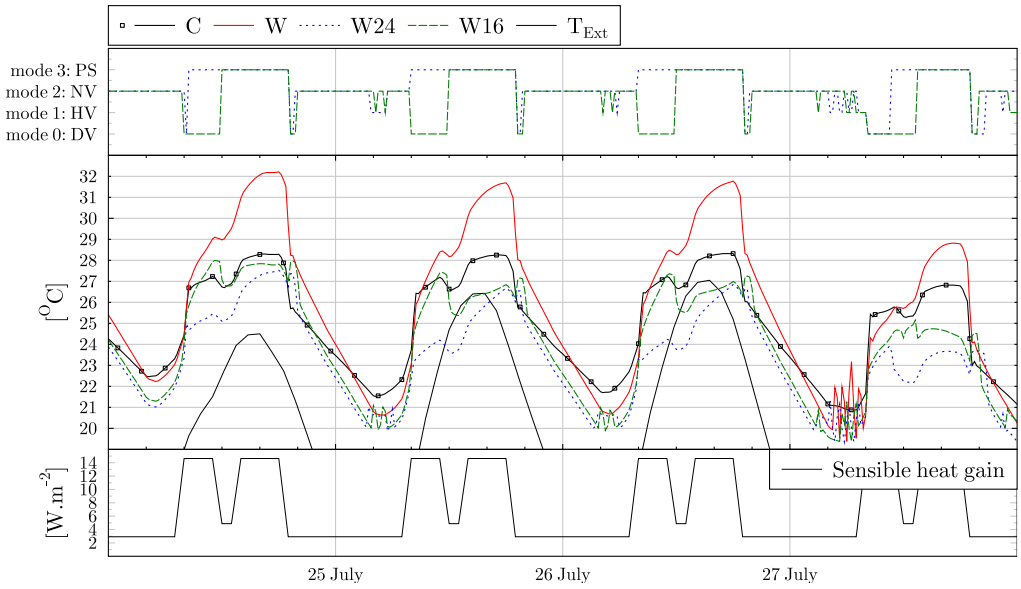

Figure 12: Internal temperature, ventilation mode for continuous and intermittent ventilation and internal load for short sequences in summer.

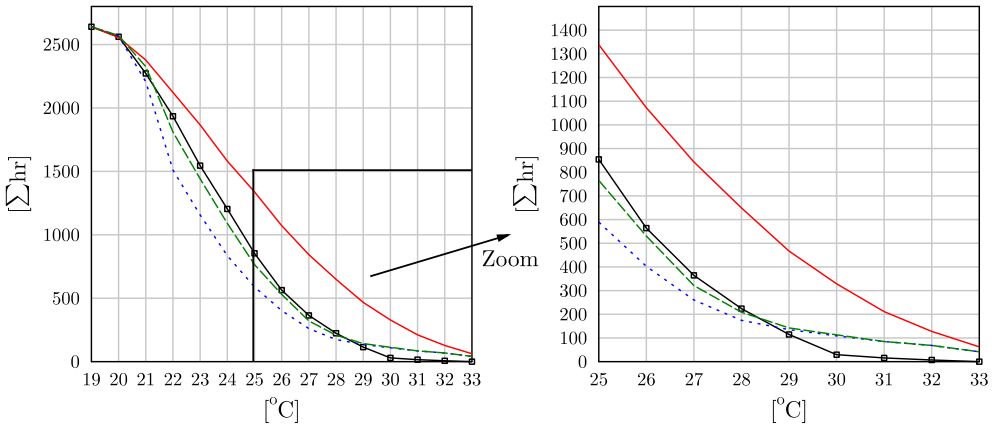

Figure 13: Number of hours exceeding a certain value for occupancy period on a one-year simulation, full-scale temperature scale on left graph and temperature higher than 25 ^oC on the right graph.

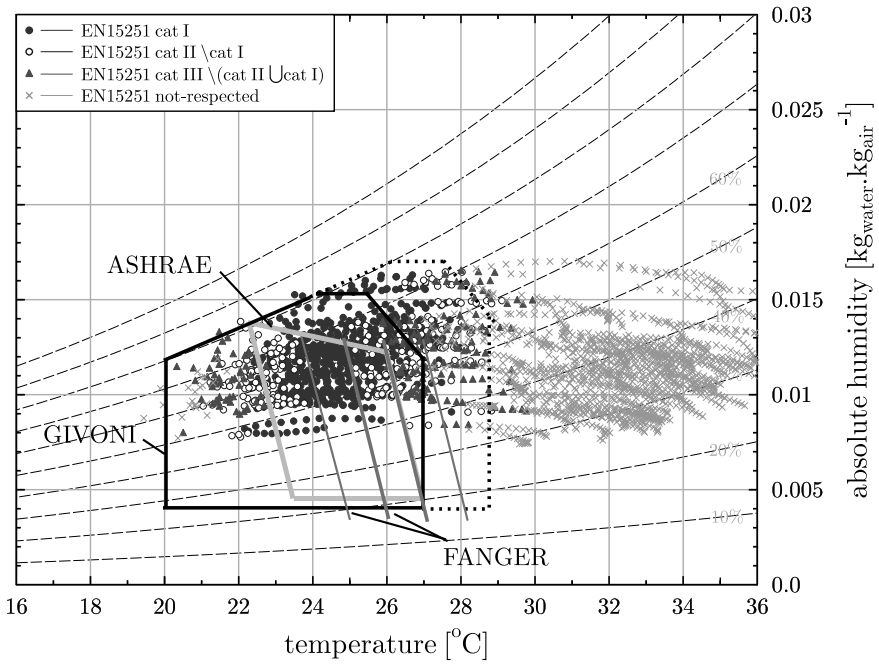

(a) W

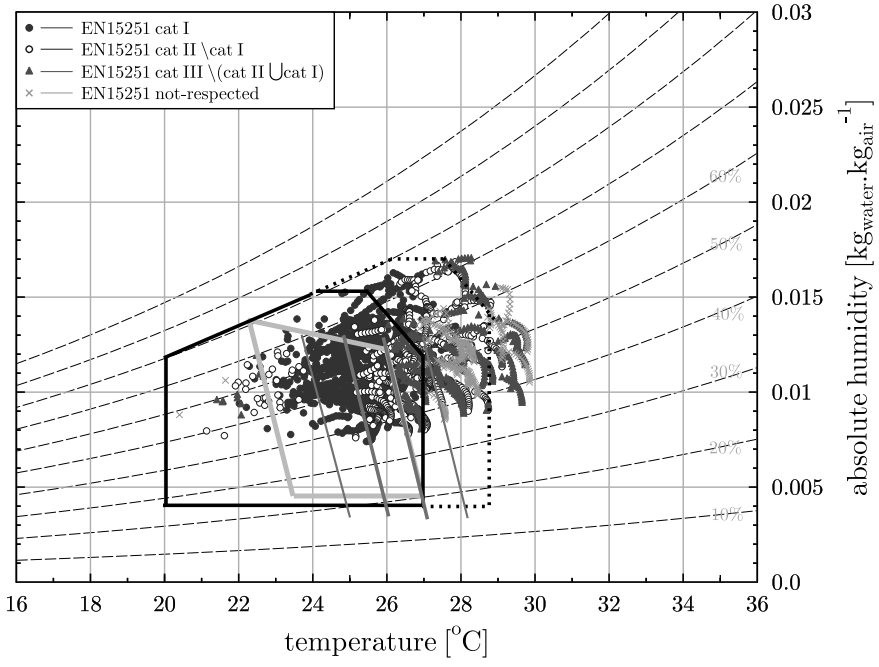

(b) Reference case : C

Figure 14: Comfort charts, (a): Night-ventilated wood structure (W), (b): Concrete structure (C).

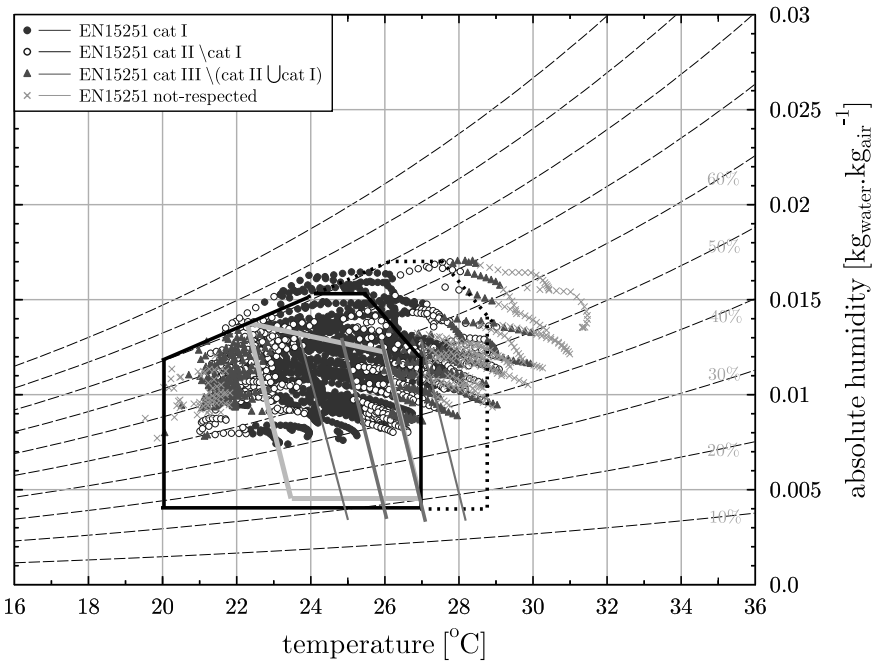

(a) W24

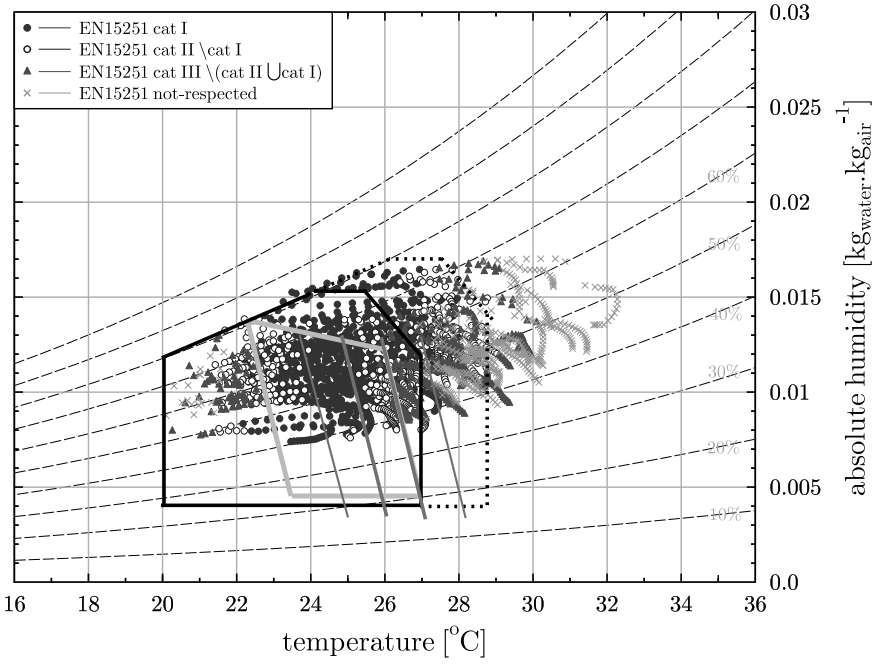

(b) W16

Figure 15: Comfort charts, (a): Wood structure associated with 24 $h/24$ HTES (W24) (b): Wood structure associated with 16 $h/24$ HTES (W16).